Theor Appl Climatol
DOI 10.1007/s00704-012-0675-1

ORIGINAL PAPER

# Parameterisation of incoming longwave radiation over glacier surfaces in the semiarid Andes of Chile

**Shelley MacDonell · Lindsey Nicholson · Christophe Kinnard**

Received: 5 September 2011 / Accepted: 14 May 2012
© Springer-Verlag 2012

**Abstract** A good understanding of radiation fluxes is important for calculating energy, and hence, mass exchange at glacier surfaces. This study evaluates incoming longwave radiation measured at two nearby glacier stations in the high Andes of the Norte Chico region of Chile. These data are the first published records of atmospheric longwave radiation measurements in this region. Nine previously published optimised parameterisations for clear sky emissivity all produced results with a root mean square error (RMSE) ~20 W $m^{-2}$ and bias within ±5 W $m^{-2}$, which is inline with findings from other regions. Six optimised parameterisations for incoming longwave in all sky conditions were trialled for application to this site, five of which performed comparably well with RMSE on daytime data <18 W$m^{-2}$ and bias within ±6 W$m^{-2}$ when applied to the optimisation site and RMSE <20 W$m^{-2}$ and bias within ±10 W $m^{-2}$ when applied to the validation site. The parameterisation proposed by Mölg et al. (J Glaciol 55:292-302, 2009) was selected for use in this region. Incorporating the proposed elevation modification into the equation reduced the bias in the modelled incoming longwave radiation for the validation site. It was found that applying the parameterisation optimised in the original work at Kilimanjaro produced good results at both the primary and validation site in this study, suggesting that this formulation may be robust for different high mountain regions.

S. MacDonell (✉) · C. Kinnard
Centro de Estudios Avanzados en Zonas Áridas (CEAZA),
Campus Andrés Bello, Raúl Bitrán s/n,
La Serena, Chile
e-mail: shelley.macdonell@gmail.com

L. Nicholson
Center for Climate and Cryosphere, Institute for Meteorology and Geophysics, University of Innsbruck,
Innrain 52,
6020 Innsbruck, Austria

## 1 Introduction

In both high latitude and high-altitude environments, radiation fluxes are typically the most important sources of energy for ablation of snow and ice surfaces (e.g. Mölg and Hardy 2004; van den Broeke et al. 2006; Hoffman et al. 2008). While shortwave radiation has often been considered the dominant energy source, energy from incoming longwave radiation (hereafter LWI) can match, or exceed, that from incoming shortwave radiation during cloudy periods (Müller 1985; Granger and Gray 1990; Duguay 1993) or when net shortwave radiation is low due to either high-surface albedo or low-incident solar radiation levels experienced in winter (Ambach 1974; Fassnacht et al. 2001). More recent work has found that in many environments LWI constitutes the greatest source of energy for snow and ice melt (Ohmura 2001; Hock 2005; Sedlar and Hock 2009). Therefore, LWI is an important component to measure, or parameterise with care, when applying energy and mass balance models to snow and ice surfaces.

In glacierised environments, logistical difficulties often restrict the distribution and maintenance of weather stations, as well as the type of instrument that can be installed, so direct measurements of LWI are sparse. Physically based calculations can be used to determine LWI based on atmospheric properties and theoretical emission values for water vapour, carbon dioxide and ozone (e.g. Charlock and Herman 1976). However, determining the effects of clouds using a theoretical approach is a complex problem and so physically based calculations of LWI are generally limited to clear sky conditions. Instead, parameterisations for LWI

Published online: 02 June 2012

have been developed to fit either clear sky conditions (e.g. Brunt 1932; Brutsaert 1975; Satterland 1979), or all sky conditions (e.g. Crawford and Duchon 1999; Sicart et al. 2006; Mölg et al. 2009), using a combination of air temperature, humidity and cloud cover variability or atmospheric transmissivity. Recent work has explored optimising parameters at specific (e.g. Sicart et al. 2010) and multiple (e.g. Flerchinger et al. 2009) locations, and has compared parameterisations for different sky conditions (e.g. Sedlar and Hock 2009). Due to a lack of available meteorological data, no previous study has identified which LWI parameterization best suites the climatic conditions in the semiarid Andes. The extreme and distinct climate setting of this high-altitude region, characterised by intense solar radiation and a very dry atmosphere punctuated by large changes in humidity, warrants a detailed study of LWI parameterisation.

Although it is generally thought that LWI does not show significant spatial variability at the local scale (Oke 1987), any such variations would be important for distributed glacier energy balance modelling used to predict runoff from glacierised catchments. Concurrent measurements from multiple LWI sensors within a catchment are rare in high-elevation regions, and due to the importance of LWI in the energy balance, both the spatial and temporal variabilities of measured LWI warrant further investigation.

Within the Pascua-Lama mining project area (29°S, 70°W) in the Norte Chico region of Chile, meteorological data are available from one to nine high-altitude (>3,500 m) automatic weather stations (AWSs) since 1999. LWI has been measured continuously at two stations installed on glacier surfaces above 5,000 m above sea level (a.s.l.) since October 2008 (Table 1; Fig. 1). The data from these two stations provide an opportunity to (1) understand how measured LWI varies over relatively short distances (~1.5 km) and seasons, in the semiarid Andes, and (2) assess which all sky LWI parameterisation is best suited for use in this region. Addressing these points will provide a better understanding of the spatial and temporal variabilities of the energy balance that dictate the rate of melt and sublimation over glacier surfaces, and using measurements from the longest on-site AWS record will enable the reconstruction of LWI back to 1999. This extended record will be used in further studies of glacier mass balance and catchment-scale meltwater discharge spanning the last decade.

## 2 Site and data description

In the upper Huasco Valley, the annual average relative humidity remains below 40 % and clear skies predominate. At 3,700 m a.s.l., 90 % of precipitation occurs between May and August (Rabatel et al. 2011), although small precipitation events can occur at high elevation in the summer (typically during January and February) due to convective activity (Vuille and Keimig 2004). Temperatures peak between December and February and, at the elevation of the lower limit of glaciation (4,112 m a.s.l.; Nicholson et al. 2010), monthly and annual mean temperatures are subzero, although positive temperatures are reached for a few hours per day during summer (Rabatel et al. 2011). The main ablation season is the austral summer (November–April), which coincides with convective storms in the high Andes (Vuille and Keimig 2004). These storms are characterised by thick cloud in the afternoon, which limits the receipt of incoming shortwave radiation and increases the relative importance of LWI as a positive flux in the energy balance. Therefore, modelling longwave radiation receipt during this period is crucial for obtaining reliable ablation model results.

**Table 1** Configuration of the AWS on each glacier, and the mean (standard deviation) recorded at each station during the measurement period (October 2008–April 2011)

| | G-AWS | T1-AWS |
|---|---|---|
| Elevation (m.a.s.l.) | 5,317 | 5,226 |
| Sky view factor[a] | 0.94 | 0.97 |
| Air temperature ($T_a$) and relative humidity (RH) sensor | Vaisala HMP45 | |
| $T_a$/RH sensor accuracy | $T_a$ 0.3°C; RH <3 % | |
| Radiation sensor | Kipp & Zonen CNR1 | |
| Radiation sensor estimated accuracy on daily total | ±10 %[b] | |
| $T_a$/RH sensor height (m) | 1.6 | 2.3 |
| Radiation sensor height (m) | 1.6 | 1.3 |
| Air temperature (°C) | −9.3 (5.6) | −9.0 (5.7) |
| Relative humidity (%) | 40.4 (26.1) | 42.3 (25.4) |
| Wind speed (m $s^{-1}$) | 9.3 (4.9) | 6.6 (3.3) |
| Incoming shortwave radiation (W $m^{-2}$) | 313 (415) | 304 (400) |
| Incoming longwave radiation (W $m^{-2}$) | 171 (40) | 181 (38) |

[a]As estimated from a digital elevation model constructed using Ikonos (2005) images in ArcGIS 9.3

[b]Studies indicate that in cold environments daily error is improved to ±5 % (van den Broeke et al. 2004; van As et al. 2005)

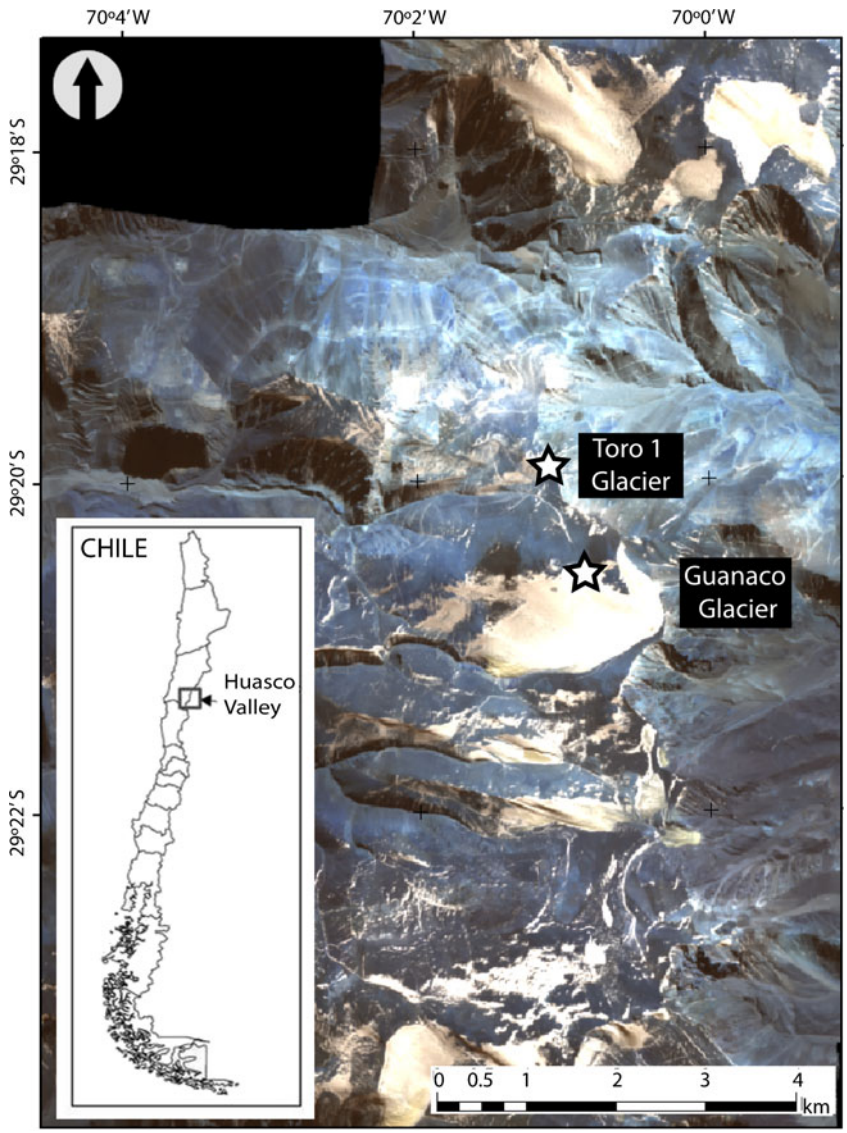


**Fig. 1** Ikonos image (2005) of the upper Huasco river catchment showing the location of the automatic weather stations (*star*) on Guanaco and Toro 1 glaciers

This study uses 2.5 years of measurements from AWSs located on two glaciers in the upper Huasco Valley, in the semiarid Norte Chico region of Chile (Table 1; Fig. 1). The primary study site is on Guanaco Glacier (29.34°S, 70.01°W, 4,985–5,350 m a.s.l.), which is a relatively large glacier for the region (1.8 km$^2$) and straddles the Chilean–Argentinian divide (Nicholson et al. 2010). Secondary observations were made on the Toro 1 Glacier (29.33°S, 70.02°W, 5,080–5,235 m a.s.l.), ~1.5 km north of Guanaco Glacier. Toro 1 is a small 'glacieret' (0.06 km$^2$) (as defined by Cogley et al. 2011); however, for simplicity it is referred to as a 'glacier' in this paper.

On both glaciers, the AWSs (hereafter G-AWS (Guanaco) and T1-AWS (Toro 1)) are equipped with a Young anemometer, a naturally ventilated Kipp and Zonen CNR1 to measure incoming and outgoing shortwave and longwave radiations, and a naturally ventilated, shielded Vaisala HMP45 to measure air temperature and relative humidity (Table 1). Campbell Scientific CR1000 data loggers scan each variable at 10 s intervals and record hourly averages. The quality of data collected from unattended sensors in harsh environments can suffer from a number of detrimental effects (Halldin and Lindroth 1992; Philipona et al. 2004; van den Broeke et al. 2004) and careful quality control is required (Box et al. 2004). In the data sets used here, all hourly averages were within expected ranges, and comparison of values from the upper and lower radiometers indicates that the readings were not adversely affected by snow cover or riming of the upper sensors over the period of study. The accuracy of radiometers reported from field studies varies depending on the instrument type and study site. Studies from cold glacier sites show even unventilated CNR1 sensors to have a daily total accuracy better than ±10 % (e.g. van den Broeke et al. 2004), while a study over grass indicates a poorer performance (Michel et al. 2008). As the AWS sensors were naturally ventilated, it is possible that measurements are affected by solar heating under coincident

high-solar radiation and low-wind conditions (Georges and Kaser 2002). However, as mean wind speed is in excess of 9 $ms^{-1}$ with 80 % of all hourly mean wind speed >5 $ms^{-1}$ and only 11 %<3.5 $ms^{-1}$, the problem is likely to be minimal at this site, and consequently no corrections were applied to the temperature or relative humidity data. The maximum effect of solar heating on longwave radiation measured by the CNR1 is 25 $Wm^{-2}$ at 1,000 $Wm^{-2}$ solar irradiance (Campbell Scientific 2011). In the absence of shaded measurements required for formal correction of any solar heating effects, no window heating offset correction was applied. Water and ice saturation vapour pressure was calculated from the measured relative humidity and air temperature using the Magnus Teten equation (Murray 1967) over ice for air temperatures <0°C and Sonntag's equation (1990) over water for air temperatures >0°C.

## 3 Methodology for assessing parameterisations of incoming longwave radiation

Assuming no additional input from the surrounding terrain, which, given the very high sky view factors at the AWS sites (Table 1) is likely to be negligible, LWI received at the surface ($L\downarrow$) can be described by:

$$L\downarrow = \varepsilon_{cs}(T,e)\sigma T^4 F \quad (1)$$

where $\varepsilon_{cs}$ is the clear sky emissivity, dependent on air temperature, $T$ (in Kelvin), and vapour pressure, $e$ (in hectopascals), of the air near the ground, $\sigma$ is the Stefan–Boltzmann constant ($5.67\times10^{-8}$ W $m^{-2}$ $K^{-4}$) and $F\geq1$ is the cloud emission factor (Sicart et al. 2010). $F=1$ indicates clear sky conditions and no effect from clouds, while F>1 indicates an increase in emissivity caused by clouds. Near-surface air temperature and vapour pressure are measured at the site and thus the two unknown factors in Eq. 1 are the clear sky emissivity and the cloud emission factor.

### 3.1 Clear sky atmospheric emissivity

Clear sky atmospheric emissivity can be approximated from measurements of air temperature, vapour pressure or both (Brutsaert 1982). One of the most commonly used algorithms is that of Brutsaert (1975):

$$\frac{L\downarrow}{\sigma T^4} = \varepsilon_{cs} = C\left(\frac{e}{T}\right)^m \quad (2)$$

where typical values of $C$ and $m$ for a standard mid-latitude atmosphere are 1.24 and 1/7, respectively (Brutsaert 1975). On glacier surfaces, the parameterisations should account for thermal inversion and cold temperatures, and, at high altitudes, parameterisations should also account for the thin atmosphere, which may cause these values to differ (Aase and Idso 1978; Yamanouchi and Kawaguchi 1984; Mölg et al. 2009; Sicart et al. 2010) or even limit the applicability of Eq. 2 (Marks and Dozier 1979). Nine of the most commonly used previously published clear sky emissivity parameterizations were selected for testing; optimised using data from G-AWS daytime, clear sky conditions were identified as those times when measured incoming shortwave radiation was equal to the theoretical maximum calculated for the surface elevation of the site and assuming unpolluted air conditions (Lhomme et. al. 2007; see Section 3.2 for more details). For these times clear sky emissivity was computed using each of the nine parameterizations, optimised by minimising the root mean square error (RMSE) between the parameterized $\varepsilon_{cs}$ and that computed from measured LWI and air temperature (Eq. 2). The performance of the nine parameterisations is assessed on the basis of their RMSE and bias.

### 3.2 Cloud emission factor

Different parameterisations for all sky LWI formulate the cloud emission factor (Eq. 1) in a variety of ways, all of which are represented by a combination of any, or all, of the following: effective cloud cover fraction, bulk atmospheric transmissivity, relative humidity, and vapour pressure. However, the majority of commonly used parameterizations include either effective cloud cover fraction or bulk atmospheric transmissivity (e.g. Maykut and Church 1973; Sicart et al. 2006, 2010).

If no cloud cover fraction measurements are available, the effective cloud cover fraction is generally calculated using formulations similar to Beer's law (e.g. Crawford and Duchon 1999; Lhomme et al. 2007; Mölg et al. 2009). In this study, the effective cloud cover fraction ($n_{eff}$) was derived as:

$$n_{eff} = 1 - \frac{SWI}{S_0} \quad (3)$$

where SWI is the amount of measured incoming shortwave radiation, where $S_0$ is the theoretical receipt of shortwave radiation under clear sky conditions at the surface following Lhomme et al. (2007). Clear sky conditions are defined as $n_{eff}=0$ while $n_{eff}>0$ represents a degree of cloudiness.

Bulk atmospheric transmissivity ($\tau_{atm}$) can also be used to infer a cloud cover index (e.g. Sicart et al. 2010) and can be calculated using:

$$\tau_{atm} = \frac{SWI}{S_{extra}} \quad (4)$$

where SWI is the amount of measured incoming shortwave radiation, and $S_{extra}$ is the amount of clear sky shortwave radiation received at the top of the atmosphere (Sicart et al. 2010).

These two derived variables form the basis for computing the cloud emission factor. An alternative means to compute LWI for all sky conditions is to circumvent the use of a cloud emission factor and instead to develop a unique relationship based on other primary near-surface atmospheric properties (e.g. Mölg et al. 2008).

The G-AWS data were used to evaluate six published parameterisations of LWI for all sky conditions, developed for multiple uses including other high elevation, glacier studies and agricultural studies. It should be noted that the parameterisations used here do not encompass all previously published parameterizations but represent either the most commonly applied, or those developed specifically for high-altitude environments, which is the focus of this work. For the primary analysis, the parameterisations were assessed using daytime data (1000–1700 hours) as some of the parameterisations require effective cloud cover, which is unknown for nocturnal hours. The optimised parameterisations were subsequently tested using data for all hours. As this study is concerned with assessing longwave parameterisations and not nocturnal cloud cover interpolation methods, no interpolation was used during the parameterisation testing, and in the second set of computations we assume cloud-free skies during the night, with the implication that parameterisations using an effective cloud cover will underestimate LWI during cloudy nights. A short discussion of the impact of using linear interpolation to estimate nighttime cloud cover is given in Section 4.5. The models were assessed on the basis of their RMSE and bias and were subsequently applied to 2.5 years of data from T1-AWS as a validation site. Based on these results, an overall best parameterisation was selected.

## 4 Measured meteorological conditions and LWI

### 4.1 Meteorological conditions

Figure 2 shows the daily averages of key meteorological parameters measured at G-AWS from 9 October 2008–30 April 2011. Seasonal variations in meteorological conditions are governed by the receipt of shortwave radiation, which is persistently close to the theoretical site maximum. Cloud cover is episodic and largely restricted to isolated convective storm events during the summer months and frontal precipitation events in the winter months (Kull et al. 2002). Air temperature for almost all days is sub-zero and the relative humidity is low (Fig. 2), which means that the potential evaporation rate is high. Wind speeds are relatively constant throughout the year with means (± standard deviation) of 9.3±4.9 $ms^{-1}$ at G-AWS and 6.6±3.3 $ms^{-1}$ at T1-AWS during the study period (Table 1). Hourly temperatures at G-AWS vary between −29.4 to 7.6°C, with an average of −9.3°C, and at T1-AWS, temperatures vary

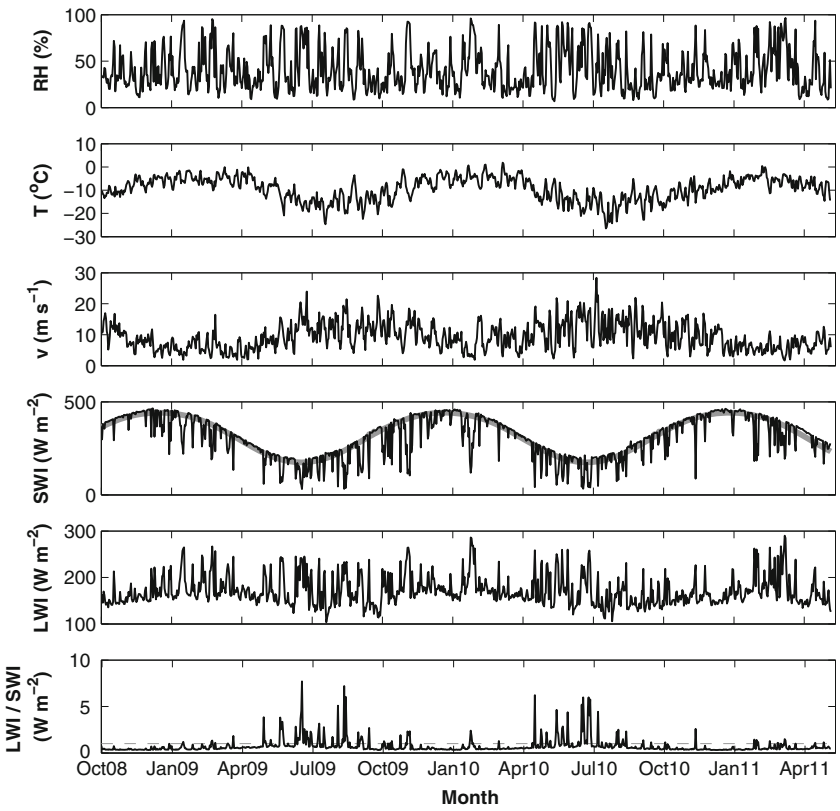


**Fig. 2** Daily (24 h) average meteorological measurements at G-AWS from 9 October 2008 to 30 April 2011. The panels show (*from the top*) relative humidity (*RH*), air temperature (*T*), wind speed (*v*), incoming shortwave radiation (*SWI*) showing the theoretical maximum SWI at surface (*grey*) and measured SWI (*black*), *LWI* and *LWI/SWI* with unity highlighted in *grey dashed line*

between −30.2 to 5.9°C with an average of −9.0°C. Mean hourly relative humidity at G-AWS (40±26 %) is slightly lower than at T1-AWS (42±25 %).

### 4.2 Measured incoming longwave radiation at G-AWS

LWI is generally low due to the high altitude and prevalence of clear sky conditions, but episodic cloud cover results in LWI receipts of up to twice that of clear sky conditions (Fig. 2) and in excess of the mean daily incoming shortwave radiation for those days. Over the whole 2.5-year study period, correlations between measured LWI and air temperature, vapour pressure and effective cloud cover are 0.023, 0.397 and 0.483, respectively (all significant at $p<0.001$), which indicate that LWI variability at the site is mainly driven by atmospheric moisture. Hence this site, with its thin and dry atmosphere owing to the high altitude, is likely to be sensitive to small vapour pressure and cloud cover variations (e.g. Vuille and Keimig 2004).

Although there is a slight seasonal temperature dependency in the baseline LWI (Fig. 2), the lack of seasonality in the humidity record means that monthly mean LWI varies little throughout the year from a minimum of 150 $Wm^{-2}$ in July to a maximum of 188 $Wm^{-2}$ in February. The relatively high mean LWI receipt during summer months is worthy of further comment, as it coincides with the main ablation season. High values of LWI are less a constant feature of the summer months but are instead driven by thick cloud cover accompanying the sporadic convective storm events during summer (Kull et al. 2002). The storms come from the eastern side of the Andes and are generally restricted to the mid-late afternoon. We approximated the frequency of convective storms by counting the number of days having more than 3 h of $n_{eff}>0.30$ during January and February, which corresponds to the months with the highest frequency of convective events. Based on this classification, convective storms occurred at G-AWS on 32 % of peak summer days between 2008 and 2011. The events were generally clustered in blocks of up to 9 days, and the highest occurrence was in 2009, when 41 % of days recorded convective conditions. The elevated LWI receipt recorded during these events (mean=224 $Wm^{-2}$) provides a stark contrast to average summertime (NDJFMA) conditions at the site (summer mean=176 $Wm^{-2}$). Driven by the minima in solar radiation, the relative importance of LWI to the net radiation budget is greatest during the winter months (MJJA), and almost all instances when daily LWI exceed daily SWI occur during these months (Fig. 2).

### 4.3 Measured clear sky emissivity at G-AWS

Daylight hours identified as having clear sky conditions ($n_{eff}=0$) were used to compute clear sky emissivity from measured LWI (Eq. 2). Clear sky emissivities over the whole measurement period typically range from 0.45 to 0.65 (Fig. 3), which is similar to dry season values from other high altitude studies (Sicart et al. 2010) but lower than values reported from glacier studies at lower altitudes where both temperature and vapour pressure tend to be higher than at G-AWS (e.g. clear sky emissivity values ranging between 0.6 and 0.85 were reported by Marty and Philipona (2000), Sicart et al. (2006) and Sedlar and Hock (2009)).

### 4.4 Drivers of LWI

LWI variability is driven primarily by cloud cover variability and humidity (Section 4.2). As there is little seasonality in humidity (Fig. 2), more detailed analysis of the drivers of LWI variation was based on data from daylight hours subdivided into clear sky- ($n_{eff}=0$) and all sky conditions. On average, the summer experienced more prevalent clear skies than the winter. The months of March and April experienced clear sky conditions for >80 % of all the daylight hours, and although June was the month with the least frequent occurrence of clear sky hours in daylight, >50 % of all daylight hours had clear sky conditions (Fig. 4).

For all clear sky hours, correlations between measured LWI and air temperature and vapour pressure (Table 2) indicate that under clear sky conditions the temperature slightly dominates the effect of vapour pressure in determining LWI

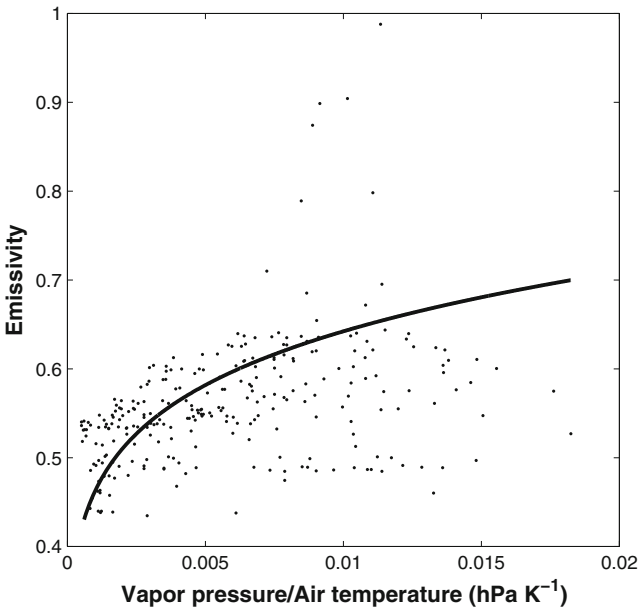


**Fig. 3** Atmospheric emissivity ($LWI/\sigma T_a^4$) versus the ratio of vapour pressure to air temperature for all daytime hourly clear sky values from 9 October 2008 to 30 April 2011. Measurements are shown by *dots*, and the *solid line* displays the result of Eq. 2, using $C=1.24$ and $m=1/7$. The large outliers are related to conditions where the emissivity is high, and the vapour pressure also increases, but not at the same relative magnitude

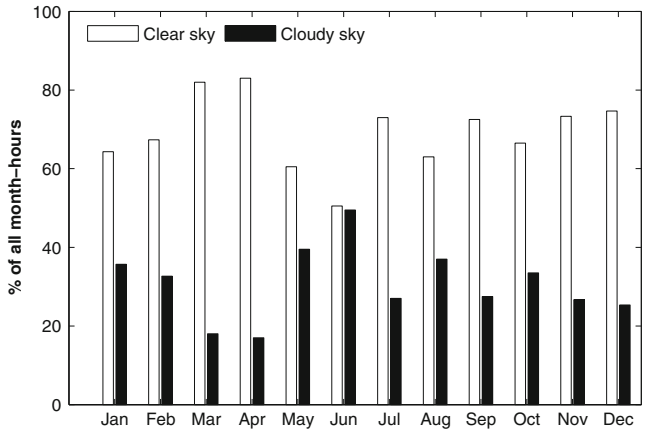


**Fig. 4** Monthly frequency of clear and cloudy sky conditions for daylight hours at G-AWS for the whole study period

fluctuations. However, whenever skies are cloudy the temperature effect is dominated by the impact of the clouds themselves and the vapour content of the atmosphere. These correlation analyses were repeated after separating the clear and cloudy sky hours into winter (MJJASO) and summer (NDJFMA) months (Table 2). Under clear sky conditions, the season does not significantly alter the correlations from the mean of the whole period, although for the first part of the study period, air temperature shows a weaker correlation with measured LWI during clear skies than in the latter part of the study period. Under cloudy skies, air temperature shows essentially no relationship to measured LWI except for in the first summer season sampled, and correlations under cloudy skies are all weaker in winter than in summer.

To calculate energy exchange at the surface, it is important to know if net incoming radiation increases or decreases with cloud formation (Ambach 1974). To assess this, total incoming all wave radiation and net all wave radiation were compared for clear sky and cloudy times. For the daylight hours of the whole study period, the mean incoming all wave radiation under clear skies is 1,082 $Wm^{-2}$, while under cloudy skies it is 766 $Wm^{-2}$. Comparatively, the net radiation under clear skies is 390 $Wm^{-2}$ compared with 198 $Wm^{-2}$ under cloudy conditions. The summer and winter seasons experience sizeable differences in incoming shortwave radiation (Fig. 2) and in the net shortwave radiation, which is also related to seasonal variations in albedo. The surface albedo fluctuates between approximately 0.35–0.45 for an ice surface and up to 0.85 for a fresh snow surface. The difference between net radiation under clear sky and cloudy sky conditions remains relatively constant (Table 3). This indicates that at this site daytime net radiation tends to decrease under cloud-covered skies compared with clear skies. More detailed analysis of this topic in conjunction with analysis of albedo is the subject of a forthcoming paper.

### 4.5 Comparison of the LWI at the two sites

Over the 2.5 years of hourly measurements, a Student's *t* test determined that LWI is significantly ($p<0.001$) different between the G-AWS and T1-AWS, with LWI being ~10 $Wm^{-2}$ higher at T1-AWS than G-AWS (Fig. 5; 95 % confidence interval 9.8–10.0 $Wm^{-2}$). As the sensors were not subjected to an inter-comparison prior to deployment, it is difficult to assess if this difference is real or associated with bias between the instruments. However, as the instrument accuracy errors (typically <10 % on daily totals; Table 1) are based on random errors, the bias between the two stations cannot be ascribed to the instrument accuracy. Further analysis was undertaken to test this apparent difference in LWI measurements between the two stations on the basis that the accuracy of these sensors in cold conditions has been shown to be better than the accuracy claimed by the manufacturer (van den Broeke et al. 2004; van As et al. 2005).

The sky view factors, which indicate differing radiative contributions from the surrounding topography, are close to

**Table 2** Correlation analyses ($p<0.001$ unless stated) between measured LWI and air temperature ($T_a$), vapour pressure ($e_a$) and effective cloud cover ($n_{eff}$) for all the study period and separated by season

| Time period | Clear hours (%) | Correlation (*r*) clear skies | | Correlation (*r*) cloudy skies | | |
|---|---|---|---|---|---|---|
| | | LWI and $T_a$ | LWI and $e_a$ | LWI and $T_a$ | LWI and $e_a$ | LWI and $n_{eff}$ |
| Whole study period 10/2008–04/2011 | 70 | 0.604 | 0.484 | 0.019 | 0.337 | 0.421 |
| Summer 2008/09 | 74 | 0.465 | 0.490 | 0.03 | 0.516 | 0.685 |
| Winter 2009 | 62 | 0.494 | 0.432 | 0.001 ($p=0.480$) | 0.216 | 0.367 |
| Summer 2009/10 | 72 | 0.643 | 0.491 | 0.001 ($p=0.598$) | 0.315 | 0.630 |
| Winter 2010 | 67 | 0.600 | 0.452 | 0.007 ($p=0.070$) | 0.235 | 0.353 |
| Summer 2010/11 | 76 | 0.607 | 0.538 | 0.012 ($p=0.044$) | 0.355 | 0.507 |

The second column indicates the percent of daytime hours which were classified as clear sky per season

**Table 3** Comparison of mean all wave radiation measured during daylight hours in the sampled seasons

| Season | Incoming all wave radiation (W m$^{-2}$) | | Net all wave radiation (W m$^{-2}$) | | Difference (W m$^{-2}$) |
|---|---|---|---|---|---|
| | Clear sky | Cloudy sky | Clear sky | Cloudy sky | Clear–cloudy |
| Summer 2008/09 | 1,255 | 990 | 476 | 286 | 190 |
| Winter 2009 | 949 | 612 | 266 | 119 | 147 |
| Summer 2009/10 | 1,141 | 891 | 423 | 273 | 150 |
| Winter 2010 | 908 | 655 | 258 | 119 | 139 |
| Summer 2010/11 | 1,176 | 877 | 450 | 247 | 203 |

unity and hence unlikely to account for the observed offset in LWI (Table 1). Instead, these results may indicate spatial variation in LWI receipt across the catchment related to differences in air temperature and vapour pressure due to the elevation difference (Gabathuler et al. 2001; Marty et al. 2002; Mölg et al. 2009), or to local scale variations in cloud cover, both of which would have implications for distributed energy balance modelling. To test this, differences in LWI were compared with differences in cloud cover, air temperature and vapour pressure between the two stations. Over the length of the record, both effective cloud cover and vapour pressure differences were significantly correlated with differences in LWI between the two sites ($r$=0.48 ($p$ <0.001) and $r$=0.39 ($p$<0.001), respectively). Separating clear and cloudy conditions showed that the difference in LWI was slightly greater under clear sky conditions, which suggests contribution from an elevation-dependent effect as well as local cloud variations.

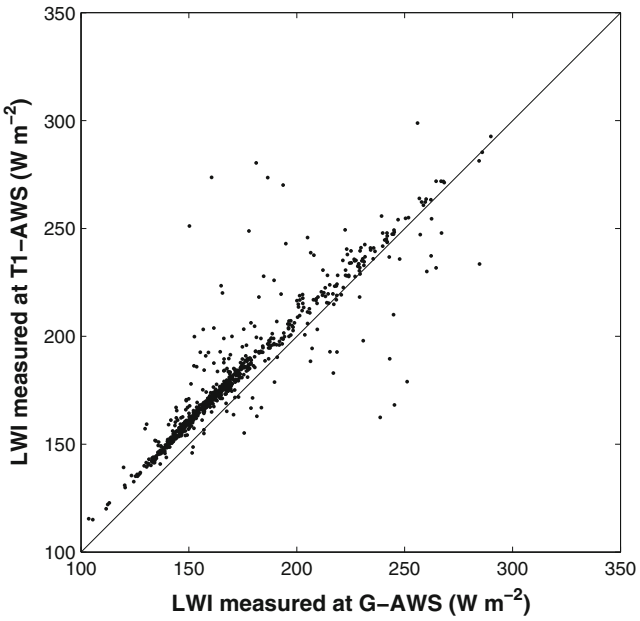


**Fig. 5** Comparison of daily average LWI measured at G-AWS and T1-AWS from 10 October 2008 to 30 April 2011. *Points* that are far off the 1:1 line may indicate different cloud cover at the two sites, but in general increasing LWI associated with cloud cover results in convergence of the measurements

## 5 Evaluation of parameterisations

### 5.1 Clear sky emissivity parameterisations for G-AWS

Results of the error analysis on the nine parameterisations tested here (Table 4) showed that the parameterisation of Brutsaert (1975) produced the best fit using the previously published parameter values (cf Fig. 3). Optimisation greatly improved the parameterisations of Ångström (1918), Brunt (1932), Swinbank (1963), Satterland (1979), Idso (1981), Prata (1996) and Dilley and O'Brien (1998), while that of Brutsaert (1975) remained relatively unchanged (Table 4). Consequently, the optimised parameterisations all performed comparably well and match the performance of the standard formula of Brutsaert. This convergence of performance across the variety of clear sky emissivity parameterisations was also found in a study on a Swedish glacier (Sedlar and Hock 2009).

The parameterisation of Brutsaert (1975) was selected to compute atmospheric emissivity in subsequent all sky LWI parameterisations, as it has been more widely used in the literature than the other models that performed equally well. The optimised $C$ value was 1.28, which is higher than that used traditionally, and higher than values used at other high-elevation sites (e.g. Lhomme et al. 2007; Mölg et al. 2009; Sicart et al. 2010). As a further test of this optimised parameter, the optimisation was rerun using the first half of the data set and validated with the second half of the hourly, clear sky values. The optimal $C$ value for the first half of the data was again 1.28, but the validation showed that the RMSE does not improve compared with using the traditional $C$ value of 1.24. As there is no physical basis to increase the value of $C$, and because there is no significant model improvement via optimisation, the original value of $C$=1.24 was retained for the LWI analysis.

If the clear sky parameterisation of Brutsaert (1975) is used to calculate LWI for the whole period, hourly all-day parameterized LWI is underestimated by 19 W m$^{-2}$ on average, and for daytime values, LWI is underestimated by 21 W m$^{-2}$ on average (Table 5). This underestimation arises because the enhancement of LWI by clouds is not taken into account in the parameterization. For individual hours, the

**Table 4** Formulae to calculate clear sky atmospheric emissivity that were tested in this study

| Source | Parameterisation | Original parameters | | Optimised parameters | | Modelled LWI (W m$^{-2}$) | |
|---|---|---|---|---|---|---|---|
| | | RMSE | Bias | RMSE | Bias | RMSE | Bias |
| Ångström (1918) | $\varepsilon_{cs} = A + B \times 10^{Ce_a}$ | 0.14 | 0.11 | 0.07 | −0.00 | 19 | 0 |
| Brunt (1932) | $\varepsilon_{cs} = A + Be_a^C$ | 0.12 | 0.09 | 0.08 | −0.01 | 23 | −3 |
| Swinbank (1963) | $\varepsilon_{cs} = AT_a^2$ | 0.13 | 0.09 | 0.09 | 0.00 | 22 | 0 |
| Brutsaert (1975) | $\varepsilon_{cs} = A\left(\frac{e_a}{T_a}\right)^{\frac{1}{B}}$ | 0.08 | −0.02 | 0.07 | 0.00 | 19 | 0 |
| Satterland (1979) | $\varepsilon_{cs} = A\left(1 - exp\left(-e_a^{\frac{T_a}{2016}}\right)\right)$ | 0.13 | 0.11 | 0.07 | 0.00 | 19 | 1 |
| Idso (1981) | $\varepsilon_{cs} = A + Be_a exp\left(\frac{1500}{T_a}\right)$ | 0.17 | 0.09 | 0.09 | 0.00 | 20 | 0 |
| Garratt (1992) | $\varepsilon_{cs} = A + Bexp(Ce_a)$ | 0.17 | 0.15 | 0.07 | −0.02 | 19 | −4 |
| Prata (1996) | $\varepsilon_{cs} = 1 - \left(1 + 46.5\frac{e_a}{6T_a}\right)exp\left(-\left(A + B\left(46.5\frac{e_a}{T_a}\right)\right)^{\frac{1}{2}}\right)$ | 0.36 | 0.30 | 0.08 | 0.01 | 19 | −2 |
| Dilley and O'Brien (1998)* | $\mathrm{LWI}_{cs} = A + B\left(\frac{T_a}{e_a}\right) + C\sqrt{1.86\frac{e_a}{T_a}}$ | 0.14 | 0.13 | 0.07 | 0.0 | 19 | 0 |

All equations use $T_a$ in Kelvin and $e_a$ in millibar. Parameters for optimisation are denoted by the capital letters A–C without subscripts. RMSE and bias for modelled emissivity are given for the equation as published in the source article and after optimisation. For comparison with other studies, we also show the error statistics on computed LWI for the clear sky conditions

[a] The Dilley and O'Brien (1998) formula was optimised for clear sky LWI and then the emissivity was back-calculated using Eq. 2 for ease of comparison with other parameterisations

underestimation can be as much as 120 W m$^{-2}$ and, in other environments that are not so dominated by clear skies, the mean discrepancy between the measured values and clear sky modelled values can be expected to be greater (Sicart et al. 2010). LWI computed by this method creates a standard against which the added value of the parameterisations for all sky conditions can be assessed.

### 5.2 All-condition LWI parameterisations and validation

Table 5 presents the results of RMSE and bias assessment of LWI calculated using the clear sky parameterisation of Brutsaert and six parameterisations for all sky conditions. The primary results are for (1) daytime data from G-AWS, which is the data set that has been used to optimise the different parameterisation equations. Supplementary to this, results are presented for each of the parameterisations applied to (2) all hourly data from G-AWS, to compare the effect of including nocturnal values, (3) daytime only and (4) all data from T1-AWS as a validation test for the optimised parameterisations.

As expected, all of the all sky LWI parameterisations improve on LWI calculated using the clear sky method. The parameterisation that circumvents the need for a cloud emission factor (Mölg et al. 2008) performs worst of the six all sky parameterisations in terms of RMSE but manages to achieve zero bias because it systematically overestimates when measured LWI is low and underestimates when measured LWI is high, suggesting that this formula does not capture the variability of LWI in the upper Huasco Valley. For the results based on the daytime G-AWS data, the lowest RMSE was obtained by the formula of Crawford and Duchon (1999), but this also had the largest bias. The remaining parameterisations are all comparable in terms of the RMSE and bias, with the formula of Mölg et al. (2009) having the lowest RMSE. The inclusion or exclusion of relative humidity data had little effect on the performance of optimised parameterisations that compute the cloud emission factor using atmospheric transmissivity (Sicart et al. 2006).

Unsurprisingly, the RMSE for modelled LWI at G-AWS increases with the inclusion of nocturnal hours for which cloud cover is unknown and the performance of Maykut and Church's formula (1973) suffers most. When applied to the secondary site, T1-AWS, the pattern of the performance of the parameterisations remains the same as was found at G-AWS, but the RMSE all increase slightly and a larger, consistently negative bias is introduced. The resultant RMSE and bias statistics of the five best performing parameterisations are inline with those found in other studies (Sedlar and Hock 2009), suggesting that these parameterisations are robust for applications in this region for which RMSE of ~10 % of the mean value is tolerable. Including all data hours into the analysis and assuming clear sky conditions at night for the T1-AWS validation site resulted in a consistently more negative bias in all the LWI parameterisations.

On the basis of these comparisons, there is little to choose between the performance of parameterisations from Sicart et al. (2006) and Mölg et al. (2009). We chose to focus further on the Mölg et al. (2009) parameterisation as it includes an optional elevation-dependant effect and because it has performed acceptably in an environment dominated by periodic development of thick convective cloud cover (Mölg et al. 2009). The improvement in modelled LWI gained by using

**Table 5** RMSE and bias (both W m$^{-2}$) results of LWI parameterisations trialled at both sites in this study

| Source | LWI parameterization | Optimised parameter (original) | G-AWS | | | | T1-AWS | | | |
|---|---|---|---|---|---|---|---|---|---|---|
| | | | Daytime | | All data | | Daytime | | All data | |
| | | | RMSE | Bias | RMSE | Bias | RMSE | Bias | RMSE | Bias |
| Brutsaert (1975) clear sky | $\varepsilon_{cs}\sigma T_a^4$ | | 37.1 | −21.0 | 39.7 | −19.2 | 39.5 | −26.5 | 42.1 | −26.0 |
| Maykut and Church (1973) | $\varepsilon_{cs}\sigma T_a^4\left(1+An_{eff}^B\right)$ | A=0.600 (0.22)<br>B=0.450 (2.75) | 17.5 | −4.5 | 45.5 | −3.1 | 19.5 | −5.2 | 25.5 | −8.2 |
| Crawford and Duchon (1999) | $\varepsilon_{cs}\sigma T_a^4\left(1-n_{eff}^A\right)+Bn_{eff}^A\sigma T_a^4$ | A=0.677 (4)<br>B=0.990 (0.952) | 15.6 | −6.0 | 24.0 | −4.5 | 17.8 | −9.2 | 24.5 | −10.5 |
| Sicart et al. (2006) | $\varepsilon_{cs}\sigma T_a^4(A+BRH+C\tau_{atm})$ | $A$=1.934 (1)<br>$B$=−0.060 (0.44)<br>$C$=−0.868 (−0.18) | 17.8 | 1.2 | 25.5 | 0.2 | 18.6 | −4.0 | 25.1 | −5.8 |
| Sicart et al. (2006) | $\varepsilon_{cs}\sigma T_a^4\left(A+B\tau_{atm}^C\right)$ | $A$=1.659 (1.5)<br>$B$=−0.617 (−7/8)<br>$C$[a]=2 (2) | 17.3 | 1.3 | 25.3 | 1.9 | 18.3 | −2.3 | 24.5 | −3.9 |
| Mölg et al. (2008) | $A+BT_a+Ce_a+DT_a^2-ET_ae_a+Fe_a^2$ | $A$=4,950.589 (6,854.2904)<br>$B$=38.044 (−58.0435)<br>$C$=6.631 (1,562.6514)<br>$D$=0.075 (0.1232)<br>$E$=0.026 (−5.9170)<br>$F$=0.010 (14.9242) | 23.6 | 0.0 | 52.3 | −34.9 | 29.6 | −19.6 | 57.6 | −44.2 |
| Mölg et al. (2009) | $\varepsilon_{cs}\sigma T_a^4\left(A+Bn_{eff}+Cn_{eff}^2+Dn_{eff}^3\right)$ | $A$=0.756 (1.0603)<br>$B$=1.715 (1.9040)<br>$C$=1.603 (-2.6560)<br>$D$=1.039 (1.3393) | 17.2 | 1.3 | 25.4 | 2.0 | 18.3 | −2.0 | 24.5 | −3.7 |

$e_a$ is water vapour pressure [in hectopascal], $T_a$ is air temperature [in Kelvin]; $n_{eff}$ is effective cloud cover fraction; $\tau_{atm}$ is atmospheric transmissivity, $\varepsilon_{cs}$ is clear sky emissivity (Eq. 2 (Brutsaert 1975) with $C$=1.24 and $m$=1/7). Parameters denoted by capital letters A–F were optimised (to 3 decimal places), and the values used in the source study are given in parenthesis

[a] This equation was optimised using linear powers in keeping with the original formula use

an all sky parameterisation is further illustrated in Fig. 6a, b. The clear sky parameterization of Brutsaert (1975) shows increasing negative discrepancy between modelled and measured LWI as measured LWI increases (Fig. 6a), while LWI modelled with the Mölg et al. (2009) parameterisation for G-AWS are closer to the measured values, but with a tendency to slightly overestimate LWI in high LWI conditions, and with residual error being largest in the mid-range of measured LWI, when partial cloud cover is the likely sky condition (Fig. 6b).

### 5.3 Elevation dependency of LWI

In order to investigate the potential elevation dependency of LWI at this site, the alternative elevation-dependent parameterization proposed by Mölg et al. (2009) was used, where the optimised cloud emission factor is modified by a denominator incorporating the ratio of mean air pressure at the computation site ($P_a$) to the mean air pressure at the reference site. Pressure was not measured at the two AWS locations but derived from standard atmospheric pressure for the station elevations giving a pressure level of 550 and 540 hPa at T1-AWS and G-AWS, respectively. This modified parameterisation was applied to the T1-AWS site and, for comparison, so was the original algorithm from Mölg et al. (2009), optimised for the reference site in their study (5,873 m on Kibo, Kilimanjaro with mean air pressure of 502 hPa):

$$\mathrm{LWI} = \varepsilon_{cs}\sigma T_a^4 \frac{\left(1.0603 + 1.9040 n_{eff} - 2.6560 n_{eff}^2 + 1.3393 n_{eff}^3\right)}{1 + n_{eff}\left(\frac{P_a}{502} - 1\right)} \quad (5)$$

Comparison of the error properties of the parameterisation remain the same when substituting the locally optimised algorithm with Eq. 5 (Fig. 6b, c) and when applied to the validation site. For the daytime data at T1-AWS, this original elevation-dependent parameterisation (Eq. 5) outperforms the version that was optimised using local data from G-AWS and in fact performs the best of all the parameterisations tested for the validation data set. The performance of Eq. 5 applied to T1-AWS is the same as the RMSE if the parameterisation is optimised directly with data from the T1-AWS station (RMSE 17.8 $\mathrm{Wm^{-2}}$; bias 1.5 $\mathrm{Wm^{-2}}$). The observed difference in measured mean LWI for daylight hours of 10 $\mathrm{Wm^{-2}}$ between G-AWS (181 $\mathrm{Wm^{-2}}$) and T1-AWS (191 $\mathrm{Wm^{-2}}$) is well simulated by both versions of the pressure-modified parameterisation, with computed daytime mean LWI of 183 and 189 regardless of whether the model was optimised at G-AWS or Kibo (Table 6). Furthermore, the results of applying Eq. 5 to data from G-AWS perform comparably well with all of the five best optimised all sky parameterisations reported in Table 5, although understandably not quite as well as the version optimised for this site. This suggests that Eq. 5 could be used without local optimisation to calculate LWI in this environment. For spatially distributed energy balance modelling over glaciers in this region, the use of Eq. 5 has the added

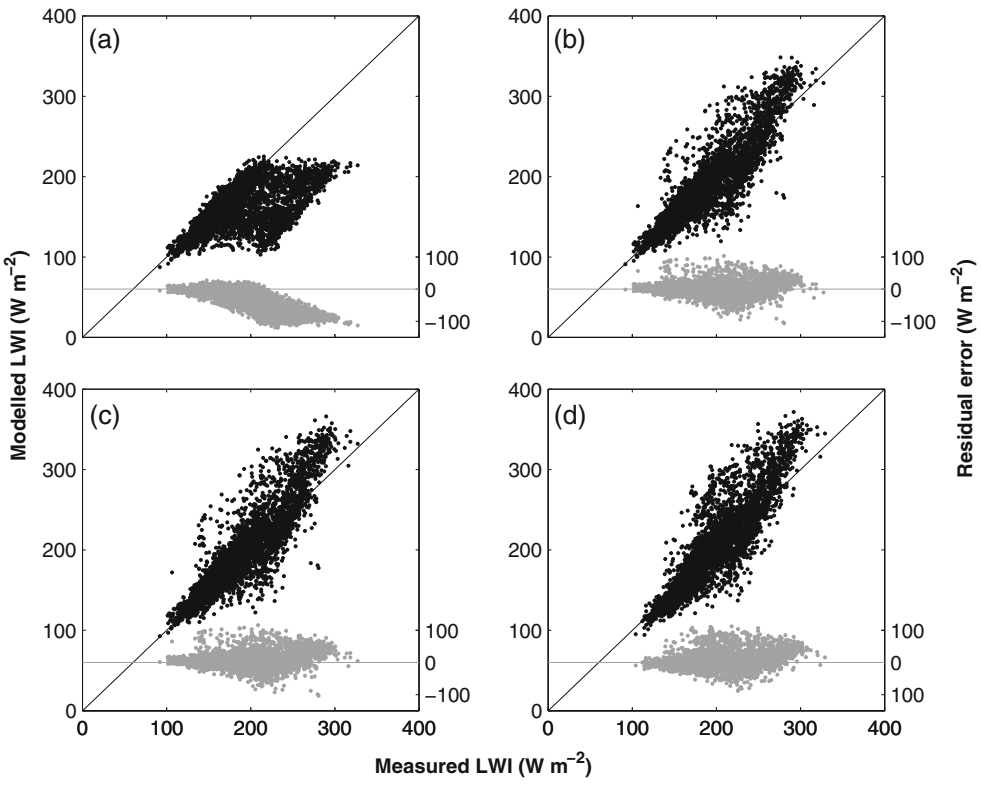


**Fig. 6** Comparison of measured and modelled LWI for daytime values (*black*) and the corresponding error as a function of measured LWI (*grey*) for **a** G-AWS using the clear sky computation of Brutsaert (1975); **b** G-AWS using the optimised all sky parameterisation of Mölg et al. (2009) without any elevation correction; **c** G-AWS; and **d** T1-AWS using the all sky parameterisation of Mölg et al. (2009) without any localised optimisation, but modified for the elevation of the respective sites

**Table 6** RMSE (in watts per square metre) and bias (in watts per square metre) results for LWI computed using an elevation corrected version of the locally optimised model of Mölg et al. (2009) and the original version of the model, optimised with data collected near the summit of Kibo, Kilimanjaro

| Parameterisation | G-AWS; daytime data | | G-AWS; all data | | T1-AWS; daytime data | | T1-AWS; all data | |
|---|---|---|---|---|---|---|---|---|
| | RMSE | Bias | RMSE | Bias | RMSE | Bias | RMSE | Bias |
| Mölg et al. (2009) optimised at G-AWS | (17.2) | (1.3) | (25.4) | (2.0) | (18.3) | (−2.0) | (24.5) | (−3.7) |
| Mölg et al. (2009) optimised at G-AWS+elevation correction | | | | | 18.6 | −1.4 | 24.6 | −3.2 |
| Molg et al. (2009) optimised at Kibo (i.e. Eq. 5) | 17.8 | 2.6 | 26.2 | 5.2 | 17.9 | −1.4 | 24.4 | −2.8 |

Values in parentheses are the same as the results presented in Table 5 and are repeated here solely to ease comparison

advantage of incorporating an elevation-dependent component which may be significant as the glaciers in this region span a wide elevation range (4,000–6,000 m a.s.l.; Nicholson et al. 2010), and measurements suggest that vertical gradients in temperature and vapour pressure at this site could be higher than those observed in other regions (Marty et al. 2002).

### 5.4 Applicability of Mölg et al. parameterisation to periods of summer storm cloud development

LWI is strongly dependent on the cloud cover conditions (Section 4.2), and hence, during cloudy times, LWI can be expected to play a more important role in the surface energy balance that dictates the rate of sublimation and melt of snow and ice surfaces. As summer is the main ablation season in the semiarid Andes, it is important to determine if the LWI parameterisation performs well during times of summer cloud development. For this purpose, the application of the elevation-dependent parameterisation optimised at Kibo (Equation 5; Mölg et al. 2009) was analysed separately for G-AWS for January 2010, which experienced the greatest cloud cover during the 2.5-year period studied (Fig. 2). For daytime values during this month, the model generally overestimates LWI with a bias of 11.7 $Wm^{-2}$ compared to only 2.6 $Wm^{-2}$ for the whole 2.5-year period. This results from the tendency of the parameterisation to overestimate when LWI is high, such as under very cloudy summer skies (Figs. 6c and 7). However, the RMSE (19.5 $Wm^{-2}$) is within the error of the measurements and similar to model performance reported in other studies (Flerchinger et al. 2009). Moreover the hourly variations capture well the main features of the measured LWI (Fig. 7), indicating that the parameterisation of Mölg et al. (2009) adequately characterises longwave radiation receipt even during thick cloud conditions which characterise summer convective events.

### 5.5 Interpolation of nocturnal cloud cover

Due to the absence of reliable information on night-time cloud cover in the extended meteorological records at the site, parameterisations have been primarily evaluated on the basis of calculated and measured LWI during daylight hours. For the 'all-day' data analysis, nocturnal cloud cover was assumed to be zero, although this is unlikely to be the case for the whole data set. However, the incorporation of a nocturnal cloud factor is unlikely to make a significant difference during the summer months, when cloud events are caused by convective storms, as Vuille and Keimig (2004) found that for the region between 15°–30°S, cold convective clouds (i.e. convective events that occur between midnight and early afternoon) occur only for 2–3 days each summer.

A potential improvement on our approach is to estimate nocturnal cloud cover by linearly interpolating cloud cover between sunset and sunrise Klok and Oerlemans (2004), but doing so had very little impact on the error statistics of LWI parameterised using Eq. 5 (Mölg et al. 2009) for either the G-AWS or T1-AWS (Guanaco: RMSE 25.8 $Wm^{-2}$, bias 3.4 $Wm^{-2}$; Toro 1: RMSE 24.4 $Wm^{-2}$, bias −2.8 $Wm^{-2}$).

## 6 Discussion and conclusions

The incident radiation in the upper Huasco Valley is typically dominated by solar radiation under predominantly clear sky conditions. On a daily scale, LWI contributions to the all wave incident surface radiation can only exceed the solar contribution during cloudy sky conditions within the winter solar minima. However, overall, cloud formation reduces all wave incident radiation even over snow and ice surfaces in this environment.

LWI variability is dominated by cloud cover and humidity and, as the seasonal variation in these parameters is weak, the seasonal oscillation of LWI is not pronounced as it is in other regions, such as the tropical Andes (Sicart et al. 2010) and the McMurdo Dry Valleys, Antarctica (Hoffman et al. 2008). Additionally, the average annual amount of measured LWI is relatively low compared to most other high-altitude environments. For example, Favier et al. (2004) found that LWI averaged 272 $Wm^{-2}$ over a glacier

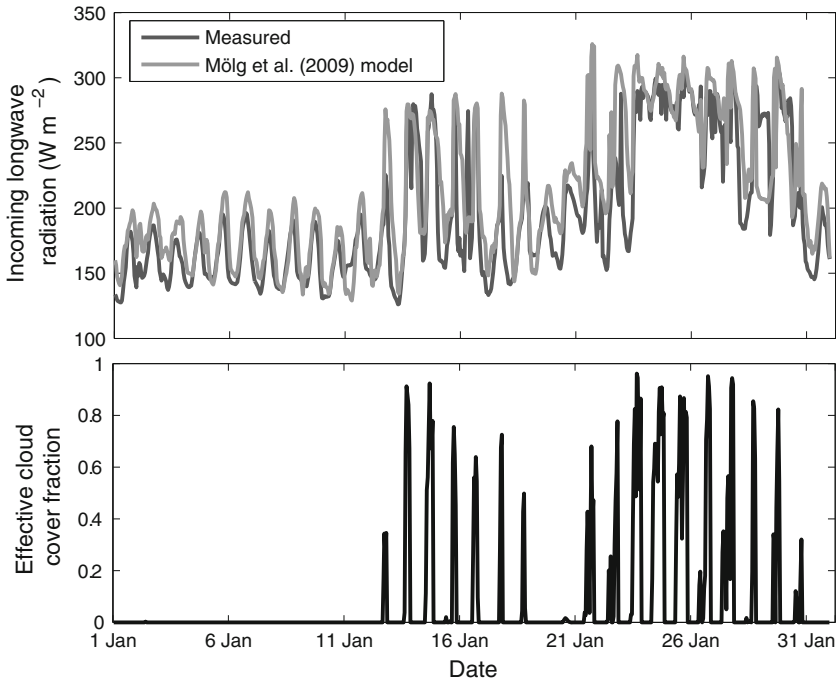


**Fig. 7** Comparison of the measured and modelled longwave radiation receipt using the Mölg et al. (2009) parameterisation offset to the elevation of G-AWS, and the corresponding effective cloud cover fraction, during January 2010

at 4,890 m a.s.l. in Ecuador and at 3,600 m a.s.l. in the upper Swiss Alps, Marty et al. (2002) recorded an annual average of approximately 220 $Wm^{-2}$ and Mölg et al. (2009) recorded a mean value of 280 $Wm^{-2}$ at 4,850 m a.s.l. over Artesonraju Glacier, Perú. These sites are all located in slightly warmer and wetter locations, where cloud formation is more prevalent, hence raising the amount of LWI received compared with the sites in this study. However, the average value recorded was similar to that recorded by Mölg et al. (2009) of 180 $Wm^{-2}$ at 5,873 on Kibo, Tanzania and the annual mean receipt of 176 $Wm^{-2}$ recorded by Hoffman et al. (2008) in the McMurdo Dry Valleys, Antarctica. The similarity in mean LWI receipt is likely due to the scarcity of cloud cover in these locations during most of the year. Whilst Kibo is in a tropical environment, the summit of Kibo generally sits above the cloud line, making contributions from cloud emission minimal at this site, and the topographic blocking of moist air from the Ross Sea near the McMurdo Dry Valleys limits cloud formation due to low vapour pressures. Comparatively, in the case at Guanaco and Toro 1 glaciers, relatively dry conditions limit cloud formation, which is similar to the case in the McMurdo Dry Valleys.

Sky emissivity derived from measurements ranges from 0.4 to 1.0, with a median value of 0.56. In keeping with previous findings (e.g. Sedlar and Hock 2009; Alados et al. 2012), all the clear sky emissivity parameterisations were found to perform comparably well, with RMSE in the order of 15 % after optimisation to the field data. The error statistics on computed clear sky LWI using these formulas are all ~20 $Wm^{-2}$ with bias within ± 5 $Wm^{-2}$ which is in the same order, or better than, other studies (e.g. Sedlar and Hock 2009; Flerchinger et al. 2009). No systematic difference in performance was evident between parameterisations using only temperature, vapour pressure or a combination of the two. This suggests that computations of LWI here can be expected to be relatively insensitive to the choice of clear sky emissivity parameterisation. This agrees with results from Flerchinger et al. (2009), who found that several unoptimised parameterizations could be used to calculate clear sky emissivity for a wide range of environment types. The optimised models presented in this study all generally performed better than the unoptimised results presented in Flerchinger et al. (2009). This suggests that whilst several parameterisation forms may be used without much variation to calculate clear sky emissivity, an exploration of site-specific parameters should always be undertaken to assess applicability (Alados et al. 2012).

LWI measured at sites separated by 1.5 km and ~90 m in elevation showed a statistically significant offset equivalent to a LWI lapse rate of −8 $Wm^{-2}$ per 100 m. Although this cannot be definitively attributed to the elevation difference rather than sensor bias, previous findings support the interpretation that this could be real. Marty et al. (2002) found that mean annual LWI decreased by 2.9 $Wm^{-2}$ per 100 m (3.3 $Wm^{-2}$ per 100 m when considering only clear sky conditions), between 370 and 3,580 m a.s.l. in the Swiss Alps, which was explained by changes of temperature (−5.5°C/km) and moisture content in the atmospheric column with elevation. Temperature and vapour pressure gradients are typically steeper at higher elevations (Mölg et al. 2009; Lhomme et al. 2007) and this is confirmed in the

upper Huasco catchment on the basis of data from two off-glacier stations (at 3,975 and 4,927 m a.s.l.) spanning a wider elevation range, which indicate that vertical gradients in air temperature and vapour pressure are −7.82°C/km and −38 Pa/km, respectively. This mean temperature lapse rate is larger than seasonal maximum lapse rates from other mountain areas (e.g. Kuhn et al. 1999; Brenning 2005). Thus, it seems plausible that the strong temperature lapse rates observed at this study site may be sufficient to drive the observed lapse rate in LWI, although further LWI measurements using inter-calibrated sensors spanning a greater elevation range within the catchment, and with comparable sky view factors, would be required to conclusively demonstrate any elevation dependency at this site.

Several parameterisations for LWI were trialled to determine which method is most suitable for use in the high Andes of the Norte Chico region of Chile. All five of the tested all sky LWI parameterisations based on clear sky emissivity and modified by a cloud emission factor provided a robust method for calculating LWI at this high-elevation site, with performance comparable to results from other studies made in different environments (e.g. Lhomme et al. 2007; Sedlar and Hock 2009; Alados et al. 2012). Their performance when applied to the validation site also produced adequate results. The all sky LWI parameterization that was based on fitting to air temperature and vapour pressure (Mölg et al. 2008) rather than using a cloud emission factor to modify clear sky LWI performed poorly, suggesting that this approach may suffer more from site specificity.

The results from all of the optimised formulas (Table 5) performed better at this site than those reported in several previous high altitude studies. For example, Flerchinger et al. (2009) reported an RMSE of between 28.9 and 31.4 W $m^{-2}$ for a range of models applied to hourly data at Nagqu, China (4,505 m a.s.l.). Their analysis included the original form of the Crawford and Duchon (1999) model, but not optimised parameterizations (they only optimised cloud corrections). Similarly, Mölg et al. (2009) report an RMSE of 27 $Wm^{-2}$ for hourly daytime data at Kersten Glacier, Kilimanjaro (5,873 m a.s.l.) and an RMSE of 27 $Wm^{-2}$ for the elevation corrected model at Artesonraju Glacier, Perú (4,860 m a.s.l.). Similarly, for hourly all-day data from Zongo Glacier, Bolivia (5,873 m a.s.l.) and Artizana Glacier, Ecuador (4,860 m a.s.l.), Sicart et al. (2010) reported RMSE values of 34 and 29 $Wm^{-2}$, respectively, for their modified version of the Sicart et al. (2006) parameterization (fifth equation in Table 5). The relatively good performance of all parameterizations at both G-AWS and T-AWS suggests that many models can be used to model LWI at this site, although models that include a cloud cover approximation perform best.

The optimised parameterisation of Mölg et al. (2009) was, by a very small margin, the best performing formula on the basis of RMSE and bias (Table 5). A modification of this formula to account for potential elevation differences was applied to a lower elevation validation site and as a result the magnitude of the negative bias in modelled LWI was reduced, although the RMSE became slightly worse. Application of the original elevation-dependent algorithm presented by Mölg et al. (2009), i.e. without optimization of the model coefficients, was found to perform satisfactorily at the primary site (G-AWS) and even better at the validation site (T1-AWS) than the locally optimised version of the model. This suggests that Eq. 5, as published in Molg et al. (2009), may be the most suitable parameterization to use for reconstructing a long-term LWI record at our site, based on measurements of air temperature, vapour pressure and incoming solar radiation made at a nearby permanent AWS since the year 1999. The assessed performance for this parameterization will further allow its application for computing distributed LWI for the glacierised surfaces of the upper Huasco catchment. Further work using an expanded set of LWI measurements from different elevations should confirm whether or not this model represents a universally suitable formula for high mountains.

Subsequent work will focus on using the data from these glaciological stations to examine the energy balances in greater detail. Given the wealth of meteorological data collected within the Pascua-Lama mining project, the Mölg et al. (2009) parameterisation could be used to produce a LWI record extending back to 1999, thereby allowing the calculation of the energy balance for the surrounding glacier surfaces over this period.

**Acknowledgments** SM was supported by FONDECYT Postdoctoral grant no. 3110053. We also thank the Barrick Gold Corporation for logistical support of this study as part of a glacier monitoring project in the semiarid Andes and the glaciology group at CEAZA for their help with the installation of the AWS's. We thank two anonymous reviewers for their constructive criticism which greatly improved this manuscript.

## References

Aase JK, Idso SB (1978) A comparison of two formula types for calculating long-wave radiation from the atmosphere. Water Resour Res 14(4):623–625

Alados I, Foyo-Moreno I, Alados-Arboledas L (2012) Estimation of downwelling longwave irradiance under all-sky conditions. Int J Climatol 32(5):781–793. doi:10.1002/joc.2307

Ambach W (1974) The influence of clouds on the net radiation balance of a snow surface with high albedo. J Glaciol 13:73–84

Ångström A (1918) A study if the radiation of the atmosphere. Smithson Misc Collect 65:1–159

Box JE, Anderson PS, van den Broeke MR (2004) Automatic weather stations on glaciers: lessons to be learned extended abstracts. In Automatic Weather Stations on Glaciers, Pontresina. pp 1-22

Brenning A (2005) Geomorphological, hydrological and climatic significance of rock glaciers in the Andes of Central Chile (33–35° S). Permafrost Periglac 16(3):231–240. doi:10.1002/ppp.528

Brunt D (1932) Notes on radiation in the atmosphere. Q J R Meteorol Soc 58:389–420

Brutsaert W (1975) On a derivable formula for long-wave radiation from clear skies. Water Resour Res 11(5):742–744

Brutsaert WH (1982) Evaporation into the atmosphere: theory, history and applications. Kluwer Academic, Dordrecht

Campbell Scientific Inc (2011) Instruction manual: CNR 1 Net Radiometer Revision 5/11

Charlock T, Herman BM (1976) Discussion of the Elsasser formulation for infrared fluxes. J Appl Meteorol 15:657–661

Cogley JG, Hock R, Rasmussen LA, Arendt AA, Bauder A, Braithwaite RJ, Jansson P, Kaser G, Möller M, Nicholson L, Zemp M (2011) Glossary of glacier mass balance and related terms, IHP-VII technical documents in hydrology No. 86, IACS Contribution No. 2, UNESCO-IHP, Paris

Crawford TM, Duchon CE (1999) An improved parameterization for estimating effective atmospheric emissivity for use in calculating daytime downwelling longwave radiation. J Appl Meteorol 38 (4):474–480

Duguay CR (1993) Radiation modelling in mountainous terrain review and status. Mt Res Dev 13:339–357

Dilley AC, O'Brien DM (1998) Estimating downward clear sky long-wave irradiance at the surface from screen temperature and precipitable water. Q J R Meteorol Soc 124A:1391–1401

Fassnacht SR, Snelgrove KR, Soulis ED (2001) Daytime long-wave radiation approximation for physical hydrological modelling of snowmelt: a case study of southwestern Ontario. IAHS Publ 270:279–286

Favier V, Wagnon P, Chazarin J, Maisincho L, Coudrain A (2004) One-year measurements of surface heat budget on the ablation zone of Antizana Glacier 15. Ecuadorian Andes J Geophys Res 109:D18105. doi:10.1029/2003JD004359

Flerchinger GN, Xaio W, Marks D, Sauer TJ, Yu Q (2009) Comparison of algorithms for incoming atmospheric long-wave radiation. Water Resour Res 45:W03423. doi:10.1029/2008WR007394

Gabathuler M, Marty CA, Hanselmann KW (2001) Parameterization of incoming longwave radiation in high-mountain environments. Phys Geogr 22(2):99–114

Georges C, Kaser G (2002) Ventilated and unventilated air temperature measurements for glacier-climate studies on a tropical high mountain site. J Geophys Res 107(D24):4775. doi:10.1029/2002JD002503

Granger RJ, Gray DM (1990) A net radiation model for calculating daily snowmelt in open environments. Nordic Hydrol 21(4–5):217–234

Halldin S, Lindroth A (1992) Errors in net radiometry: comparison of six radiometer designs. J Atmos Ocean Technol 9 (6):762–783

Hock R (2005) Glacier melt: a review of processes and their modelling. Prog Phys Geogr 29(3):362–391. doi:10.1191/0309133305pp453ra

Hoffman MJ, Fountain AG, Liston GE (2008) Surface energy balance and melt thresholds over 11 years at Taylor Glacier, Antarctica. J Geophys Res 113(F04014). doi:10.1029/2008JF001029

Idso SB (1981) A set of equations for full spectrum and 8–14 μm and 10.5–12.5 μm thermal radiation from cloudless skies. Water Resour Res 17:295–304

Klok EJ, Oerlemans J (2004) Modelled climate sensitivity of the mass balance of Morteratschgletcher and its dependence on albedo parameterization. Int J Climatol 24:231–245

Kuhn M, Dreiseitl E, Hofinger S, Markl G, Span N, Kaser G (1999) Measurements and models of the mass balance of Hintereisferner. Geogr Ann A 81(4):659–670

Kull C, Grosjean M, Veit H (2002) Modeling modern and late Pleistocene glacio-climatological conditions in the north Chilean Andes (29–30°S). Clim Change 52:359–381

Lhomme JP, Vacher JJ, Rocheteau A (2007) Estimating downward long-wave radiation on the Andean Altiplano. Agric For Meteorol 145(3–4):139–148

Marks D, Dozier J (1979) A clear-sky longwave radiation model for remote alpine areas. Arch Met Geoph Biokl, Ser B 27:159–187

Marty C, Philipona R (2000) The clear-sky index to separate clear-sky from cloudy-sky situations in climate research. Geophys Res Lett 27(17):2649–2652

Marty C, Philipona R, Fröhlich C, Ohmura A (2002) Altitude dependence of surface radiation fluxes and cloud forcing in the alps: results from the alpine surface radiation budget network. Theor Appl Climatol 72(3–4):137–155

Maykut GA, Church PE (1973) Radiation climate of Barrow, Alaska, 1962–1966. J Appl Meteorol 12:620–628

Michel D, Philipona R, Ruckstuhl C, Vogt R, Vuilleumier L (2008) Performance and uncertainty of CNR1 net radiometers during a one-year field campaign. J Atmos Ocean Technol 25:442–451. doi:10.1175/2007JTECHA973.1

Mölg T, Hardy DR (2004) Ablation and associated energy balance of a horizontal glacier surface on Kilimanjaro. J Geophys Res 109 (D16104). doi:10.1029/2003JD004338

Mölg T, Cullen N, Hardy DR, Kaser G, Klok L (2008) Mass balance of a slope glacier on Kilimanjaro and its sensitivity to climate. Int J Climatol 28:881–892. doi:10.1002/joc.1589

Mölg T, Cullen N, Kaser G (2009) Solar radiation, cloudiness and longwave radiation over low-latitude glaciers: implications for mass balance modelling. J Glaciol 55(190):292–302

Müller H (1985) On the radiation budget in the Alps. Int J Climatol 5 (4):445–462

Murray FW (1967) On the computation of saturation vapor pressure. J Appl Meteorol 6:203–204

Nicholson L, Marín J, Lopez D, Rabatel A, Bown F, Rivera A (2010) Glacier inventory of the upper Huasco valley, Norte Chico, Chile: glacier characteristics, glacier change and comparison with central Chile. Ann Glaciol 50(53):111–118

Ohmura A (2001) Physical basis for the temperature-based melt-index method. J Appl Meteorol 40(4):753–761

Oke TJ (1987) Boundary layer climates. Methuen, London

Philipona R, Dürr B, Marty C, Ohmura A, Wild M (2004) Radiative forcing—measured at Earth's surface—corroborate the increasing greenhouse effect. J Geophys Res 31(N3):L03202

Prata AJ (1996) A new long-wave formula for estimating downward clear-sky radiation at the surface. Q J R Meteorol Soc 122:1127–1151

Rabatel A, Castebrunet H, Favier V, Nicholson L, Kinnard C (2011) Glacier changes in the Pascua-Lama region, Chilean Andes (29° S): recent mass-balance and 50-year surface-area variations. Cryosphere 5:1029–1041

Satterland DR (1979) An improved equation for estimating long-wave radiation from the atmosphere. Water Resour Res 15(6):1649–1650

Sedlar J, Hock R (2009) Testing longwave radiation parameterisations under clear and overcast skies at Storglaciären, Sweden. Cryosphere 3(1):75–84

Sicart JE, Pomeroy JW, Essery RLH, Bewley D (2006) Incoming longwave radiation to melting snow: observations, sensitivity, and estimation in northern environments. Hydrol Process 20 (17):3697–3708

Sicart JE, Hock R, Ribstein P, Chazarin JP (2010) Sky longwave radiation on tropical Andean glaciers: parameterisation and sensitivity to atmospheric variables. J Glaciol 56(199):854–860

Sonntag D (1990) Important new values of the physical constants of 1986, vapor pressure formulations based on the ITC-90, and psychrometer formulae. Z Meteorol 40:340–344

Swinbank WC (1963) Long-wave radiation from clear skies. Q J R Meteorol Soc 89:339–348

van As D, van den Broeke MR, Reijmer CH, van de Wal RSW (2005) The summer surface energy balance of the high Antarctic Plateau. Bound-Lay Meteorol 115:289–317

van den Broeke MR, van As D, Reijmer CH, van de Wal RSW (2004) Assessing and improving the quality of unattended radiation observations in Antarctica. J Atmos Ocean Tech 21(9):1417–1431

van den Broeke M, Reijmer C, van As D, Boot W (2006) Daily cycle of the surface energy balance in Antarctica and the influence of clouds. Int J Climatol 26(12):1587–1605

Vuille M, Keimig F (2004) Interannual variability of summertime convective cloudiness and precipitation in the Central Andes derived from ISCCP-B3 data. J Clim 17:3334–3348

Yamanouchi T, Kawaguchi S (1984) Longwave radiation balance under a strong surface inversion in the Katabatic wind zone, Antarctica. J Geophys Res 89(D7):11771–11778